 CMES, vol.5, no.1, pp.81-90, 2004

Numerical Study of Indentation Delamination of Strongly Bonded Films by Use of a Cohesive Zone Model

W. Li[1] **and T. Siegmund**[1]

Abstract: Results of a computational study of the mechanics of indentation induced interface delamination are described for a system consisting of a ductile film on an elastic substrate. Special attention is paid to the properties of the interface between film and substrate, and the influence of the interface properties on the indentation response. Specifically, strong interfaces are considered. The interface is characterized by the use of a cohesive zone model. The finite element method is used to solve the boundary value problem, with the interface behavior incorporated via a cohesive model in a traction-separation formulation. The model does not include any initial defects and the formation of the indentation-induced delamination is accounted for in the model. While for weak interfaces buckling of the film occurs, for strong interfaces mode II delamination at the interface dominates and can be connected to pop-in events. The investigation describes a scheme such that indentation experiments can be used to determine the properties of the film-substrate interface even for strong interfaces.

keyword: Indentation, FEM, Cohesive zone model, Thin film coating.

1 Introduction

Thin film coatings are used in a series of applications of technological interest. Hard coatings on soft substrate protect the underlying material against wear. Ductile films on ceramic substrate are a common feature of semiconductor devices or optics applications. The reliability of the interface between film and substrate is critical since interface failure could cause the failure of the coating system even the coating itself does not yet fail. Indentation is one of the most widely used and best-documented methods to characterize the mechanical properties of the coating system. Recently, indentation techniques have not only been applied to identify the properties of thin films coatings, but also to determine the toughness of thin film-substrate interfaces [Marshall and Evans (1984), Volinsky, Moody and Gerberich (2002)] Several failure modes were identified that can occur during indentation of a film-substrate system. Specifically, for a ductile film on an elastic substrate, failure modes include plastic deformation of the film, delamination and film buckling. The mechanics of these failure modes must be considered if indentation results are used to determine the film material, or interface properties.

Most investigations on interface toughness measurements by use of indentation loading were focused on systems with very weak interfaces in which film buckling occurs. Based on the method proposed by Marshall and Evans (1984), the change in strain energy before and after buckling is used to derive expressions for the energy release rate at the interface. The application of this method is summarized in Volinsky, Moody and Gerberich (2002). Indentation tests have been much less successful in cases where the interface is strong [Kriese, Gerberich and Moody (1999a)] due to the large amount of plastic deformation present. While for the weak interfaces the plastic deformation of the ductile film occurs only locally at the indenter, for strong interfaces plastic deformation is present over large areas of the film. Thus both, the debonding at the interface as well as the plastic deformation of the film contribute to the delamination resistance. Since requirements of small scale yielding are not fulfilled in this case, classical fracture mechanics concepts cannot be used to derive expressions for the interface toughness.

From many past studies it is well known that solutions to fracture problems under large-scale yielding conditions can be obtained if constitutive laws both for the irreversible deformation of the solid as well as for the material separation process are used in the analysis such that both energy-dissipating mechanisms are accounted for [Tvergaard and Hutchinson (1996), Zhang, Klein,

[1] Purdue University, West Lafayette, IN, U.S.A.

Huang, Gao, Wu (2002), Chandra and Shet (2004)]. Such an approach is also attractive since no assumptions regarding the presence of initial delaminations are necessary. In the present paper, the processes of the initiation of the indentation-induced delamination and its growth are accounted for by the use of a cohesive zone model. Whether the film subsequently buckles, or grows as a shear delamination, is the direct outcome of the computational analysis and dependent on the interface properties only.

The cohesive zone model approach was used in investigations of indentation-induced delaminations in system with a hard film on an elastic-plastic substrate by Abdul-Baqi and van der Giessen (2001ab, 2002). Both interface delamination, and film cracking were considered. In Zhang, Zeng and Thampurum (2001), some simulation results were presented both for the case of an elastic film on a ductile substrate as well for a ductile film on an elastic substrate. So far, however, no systematic investigation of a ductile film-elastic substrate system has been reported such that the influence of the cohesive zone parameters characterizing the interface on the indentation response is documented.

In the present paper, results of a systematic numerical study of indentation induced interface delamination for a system consisting of a ductile film on an elastic substrate are described. Within the model approach, the interface is characterized by the parameters cohesive strength and cohesive length. The influence of these properties on the indentation response, including delamination onset, film buckling and delamination growth, is assessed.

2 Model definition

A film–substrate indentation system with a cone indenter in an axisymmetric configuration is considered in the investigation. The geometry and the boundary conditions of the model system are shown in Fig. 1. The boundary conditions applied are such that at the bottom of the elastic substrate $u_z(r)$=0. Axisymmetric conditions with $u_r(z)$=0 are applied at r=0. Loading is performed under displacement-controlled conditions with the indentation depth of the indenter tip, h, to be at maximum 1.5 times the film thickness.

The thin film coating has a thickness t and is modeled as standard isotropic elastic-plastic material. The elastic properties of the film are E_f=128 GPa, ν_f=0.34. The yield strength, σ_y=0.005E_f and a von-Mises yield criterion is used. Linear hardening is assumed for the film, with the hardening modulus as H_f=0.03E_f. The substrate is considered as isotropic elastic solid with E_s=100 GPa, and ν_s=0.25. The substrate domain considered is of size $100t \times 100t$. The indenter is assumed as rigid body, and possesses an angle of 144°. A master-slave contact mechanism is applied between indenter and film. No friction, and small sliding is considered.

The interface between film and substrate is modeled by the use of a cohesive zone model. This allows the simulation of crack initiation and growth without the introduction of any initial defects. The behavior of the interface is thereby described by a constitutive framework connecting the tractions between film and substrate to the separation between them. By adopting such a traction-separation law, crack initiation, crack propagation and film buckling become results of the stress and strain fields caused by indentation.

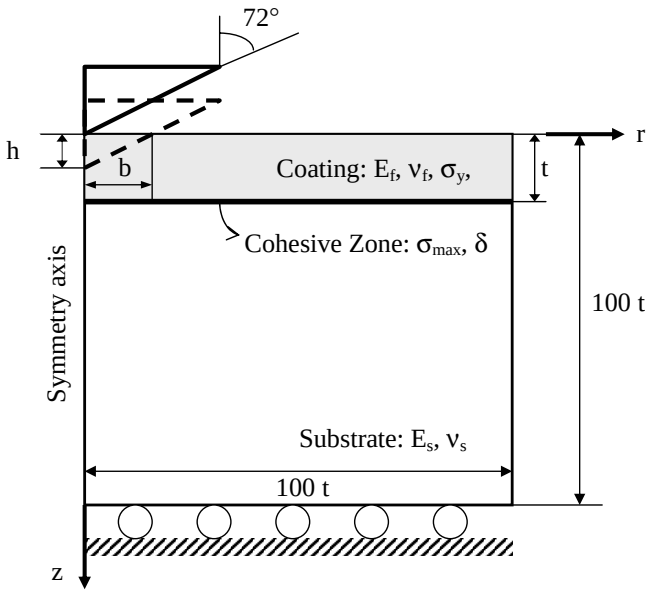

Figure 1 : Model geometry and boundary conditions

The traction-separation law for the description cohesive zone is based on a potential, ϕ:

$$\phi = \phi_c - \phi_c(1+\lambda)\exp(-\lambda) \tag{1}$$

where the cohesive energy, ϕ_c, i.e. the work required for the creation of new crack surface, is given by:

$$\phi_c = e\sigma_{\max}\delta \tag{2}$$

The cohesive zone parameters are σ_{max} and δ, the cohesive strength and length, respectively. The quantity λ designates an effective normalized displacement jump across the interface:

$$\lambda = \sqrt{\left(\frac{\Delta u_n}{\delta}\right)^2 + \left(\frac{\Delta u_t}{\delta}\right)^2} \tag{3}$$

with Δu_n and Δu_t the normal and tangential displacement jumps across the interface. Normal and tangential tractions, T_n and T_t, are obtained as derivative of the cohesive zone potential with respect to the displacement jumps:

$$\begin{aligned} T_n &= \frac{\partial \phi}{\partial \Delta u_n} = \sigma_{\max}\left(\frac{\Delta u_n}{\delta}\right)\exp(1-\lambda) \\ T_t &= \frac{\partial \phi}{\partial \Delta u_t} = \sigma_{\max}\left(\frac{\Delta u_t}{\delta}\right)\exp(1-\lambda) \end{aligned} \tag{4}$$

Also, the resulting traction, T, is given as

$$T = \sqrt{T_n^2 + T_t^2} = \frac{1}{\delta}\frac{\partial \phi}{\partial \lambda} = \lambda \sigma_{\max}\exp(1-\lambda) \tag{5}$$

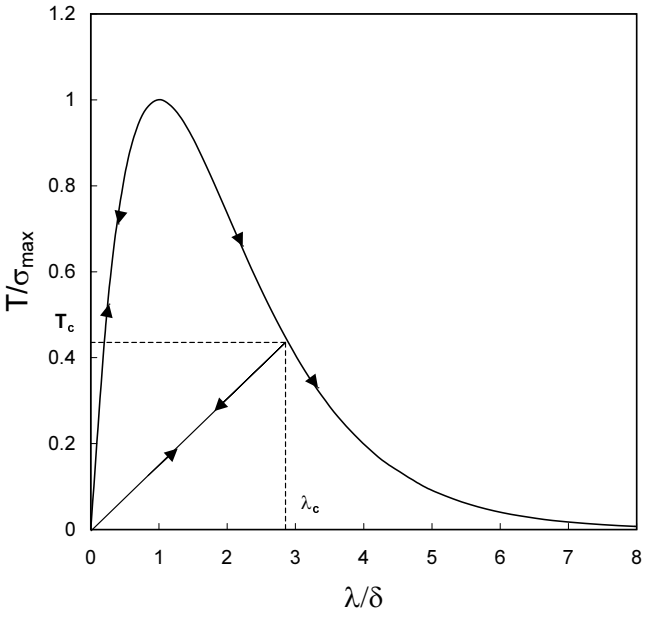

Figure 2 : The traction-separation law.

The traction-separation relationship is depicted in Fig. 2. For the cohesive zone model selected for this study, the cohesive zone material parameters are identical for normal and tangential separation. A new, traction free surface is created if $\lambda \approx 5\delta$. This condition λ=5δ then defines the location of the tip of the delamination. The smooth shape of the exponential $T-\lambda$ relationship is numerically advantageous in the present simulations where crack nucleation is accounted for.

An irreversible unloading path is included in the traction-separation formulation such that healing of delaminations during unloading events is excluded. The unloading behavior used in the present formulation is motivated by results from the framework of continuum damage mechanics [Lemaitre (1996)]. If the effective normalized displacement jump is less than the cohesive length, $\lambda < \delta$, the cohesive zone law remains reversible and unloading occurs by the traction-separation relations given in Eq. 5. No permanent damage is caused to the interface. For $\lambda > \delta$ an irreversible unloading path is used such that unloading occurs to the origin of the T-λ space as described by:

$$T = \frac{T_c}{\lambda_c}\lambda = \sigma_{\max}\lambda\exp(1-\lambda_c) \tag{6}$$

where T_c, λ_c are the resulting traction and effective normalized displacement jump at the point where unloading starts (Fig. 2). Due to this unloading path only part of the cohesive energy is recovered during unloading.

In the traction-separation law in Eq. 5, separation ($\Delta u_n > 0$) and compression ($\Delta u_n < 0$) are not distinguished from each other. To avoid issues with potential interpenetration of film and substrate, a contact surface is added to the cohesive zone model formulation between the film and substrate. With this model set-up, negative values of the displacement jump across the crack, $\Delta u_n < 0$, are essentially excluded. Under compressive loading the effective normalized displacement jump across the interface then only depends on the value of Δu_t.

Simulations are performed using the commercial finite element software ABAQUS. During the indentation simulation, the displacement of the indenter is controlled. The cohesive zone elements are implemented into this code using the user-defined element (UEL) interface. Axisymmetric (interface) cohesive elements possessing four nodes and two integration points are used in the analysis. Four-noded axis-symmetric continuum elements (CAX4) are used to model film and substrate. A typical model that leads to converged results with respect to the element size possesses a total of 2656 axisymmetric elements and 199 cohesive zone elements. The smallest element size

($l = t/5$) is used in the area close to the indenter, and the element size gradually increases with r. The modified Riks method is applied to overcome numerical difficulties due to the global unloading caused by interface failure.

3 Results

3.1 Computations

Simulations of the indentation response are performed with focus on strong interfaces. The main body of results is obtained for film-substrate systems in which the cohesive strength is between σ_{max}/σ_y=0.5 to 3.0, with the cohesive length in the range of δ/t=0.01 to 0.16. Considering these parameters, the normalized cohesive energies considered are between $\phi_c/(e t\sigma_y)=(\delta/t)(\sigma_{max}/\sigma_y)$=0.01 and 0.32. Representative for the computations performed with these parameters, Fig. 3a and b depict contour plots obtained with σ_{max}/σ_y=2.5 and δ/t=0.02. These plots show the plastic zone and the location of the interface delamination (see the arrows in the contour plots) shortly after the initiation of the delamination (Fig. 3a) and at maximum indentation depth (Fig. 3b). The plastic zone is characterized by the condition that the accumulated equivalent plastic strain is larger than 1×10^{-4}. It is evident from these plots that the tip of the delaminations is located within the plastic zone, and that small-scale yielding conditions are not fulfilled. Only a small amount of delamination occurs.

For comparison, results for the indentation response of a system with a weakly bonded interface with σ_{max}/σ_y=0.025 and δ/t=0.005 are presented. For the weak interface, contour plots for the plastic zone are depicted for the instance shortly after delamination initiation (Fig. 3c) and for maximum indentation depth (Fig. 3d). While initially the delamination is within the plastic zone, at maximum indentation depth and after film buckling the length of the delamination is considerable larger, and the tip of the delamination is outside the plastic zone. Buckling of the film leads to a considerable lift-off of the film from the substrate.

Predicted load-indentation depth ($P-h$) curves are depicted in Fig. 4a for several values of σ_{max}/σ_y under constant δ/t. The response of the weakly bonded interface is included for comparison. The indentation depth values are normalized by the film thickness. Computed values of P are normalized by the load at maximum in-

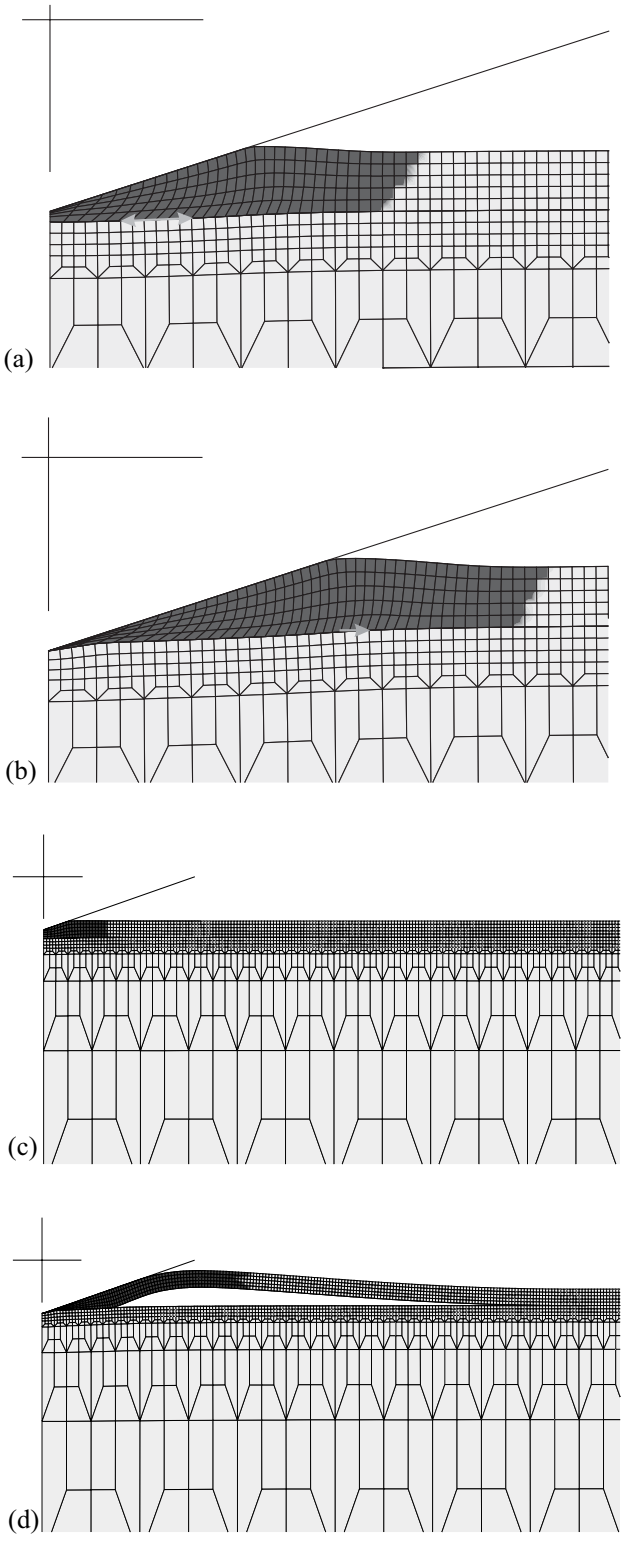

Figure 3 : Contour plots of plastic zone for σ_{max}/σ_y = 2.5 and $\delta/t = 0.02$ at (a) $h = t$ and (b) $h = 1.5t$, as well as for $\sigma_{max}/\sigma_y = 0.025$ and $\delta/t = 0.005$ at (c) $h = 0.3t$ and (d) $h = 1.5t$.

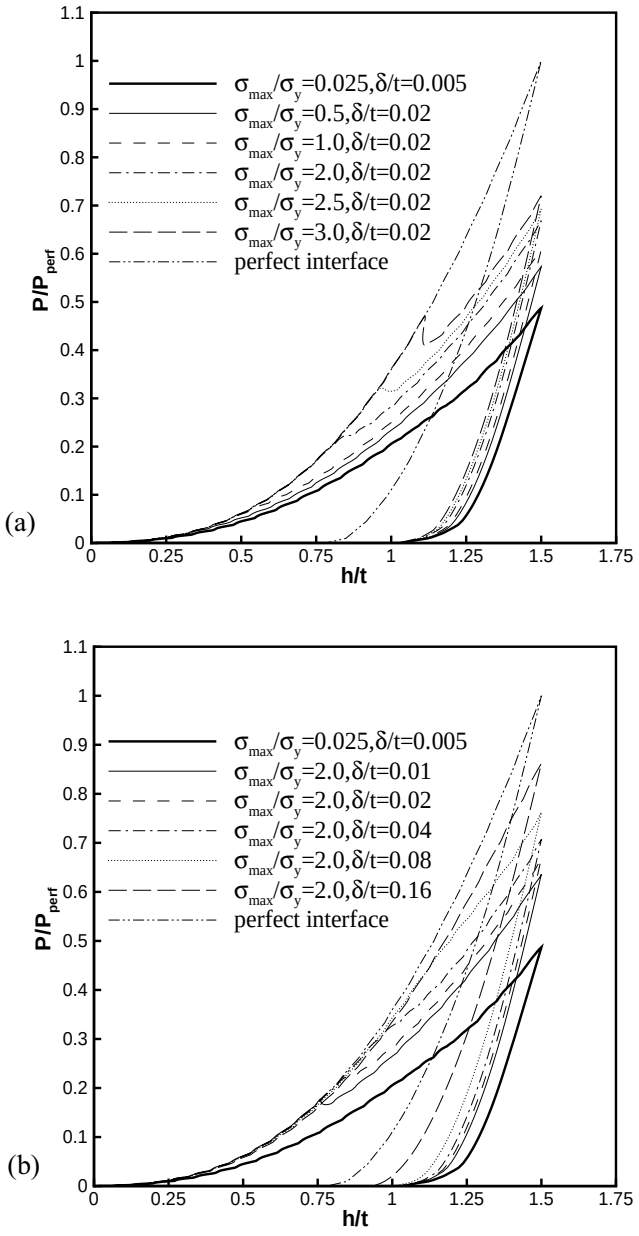

Figure 4 : Computed load indentation curves for (a) δ/t=0.02 and various values of σ_{max}/σ_y, (b) σ_{max}/σ_y=2.0 and various values of δ/t. A weak interface, σ_{max}/σ_y=0.025 and δ/t=0.005, is included for comparison.

dentation depth as obtained in a computation for a model with a perfect interface. In the perfect interface case, the nodes on the two sides of the interfaces are constrained such that the displacement jumps across the interface are zero. For the strong interfaces, the $(P-h)$ response initially follows the response for the perfect interface, $(P-h)_{\text{perf}}$. Subsequently, the $(P-h)$ curves start to deviate from $(P-h)_{\text{perf}}$ and further indentation takes place along $(P-h)$ curves with reduced slope. Deviation from $(P-h)_{\text{perf}}$ occurs early on if (σ_{max}/σ_y) is small. For stronger interfaces the $(P-h)$ curves follow those of the perfect interface to higher indentation loads. If the interface possesses $\sigma_{max}/\sigma_y > 2$, a sudden departure from $(P-h)_{\text{perf}}$ occurs, which is characterized by a pop-in event with a reduction in load. Similar results were obtained in indentation experiments in e.g. in Malzbender and de With (2000) for systems with compliant polymeric coatings on glass surfaces. The peak loads remain all above $0.5P_{\text{perf}}$, but even for the strongest interface a considerable drop in P_{max} occurs from the perfect to the strongly bonded interfaces.

For cases with the weak interface the predicted $(P-h)$ response deviates from the $(P-h)_{\text{perf}}$ very early on. The predicted $(P-h)$ curve is smooth despite that fact that the contour plots clearly show that a film-buckling event occurs. While the properties of the weak interface are considerably different from the other interface properties assumed, the maximum load of the $(P-h)$ response is not very different from those for the strong interfaces. During unloading, all cohesive zone parameter combinations result in similar unloading slope at P_{max}, and finally lead to identical amounts of residual indentation.

Figure 4b depicts the $(P-h)$ response for systems for several values of δ/t and constant σ_{max}/σ_y=2.0. As the cohesive length is increased only small changes in the load level occur at which the $(P-h)$ response deviates from $(P-h)_{\text{perf}}$. Nevertheless, the subsequent slope of the $(P-h)$ response depends on the cohesive length. Small cohesive lengths lead to smaller slopes than larger δ values, and thus to smaller maximum indentation loads. The residual indentation after unloading is found to be dependent on the cohesive length, with small values of δ leading to larger residual indentations. Again, the weak interface, despite its considerable difference in cohesive zone properties, does not possess a very different $(P-h)$ response.

Figure 5a shows the development of the interface delaminations for the simulations with δ/t=0.02 and various values of σ_{max}/σ_y. For the strong interfaces, the initiation of the delamination occurs at indentation depths, $h/t > 0.5$. The delamination initiates at $r = t$, with the location of delamination initiation moving outward as the σ_{max}/σ_y

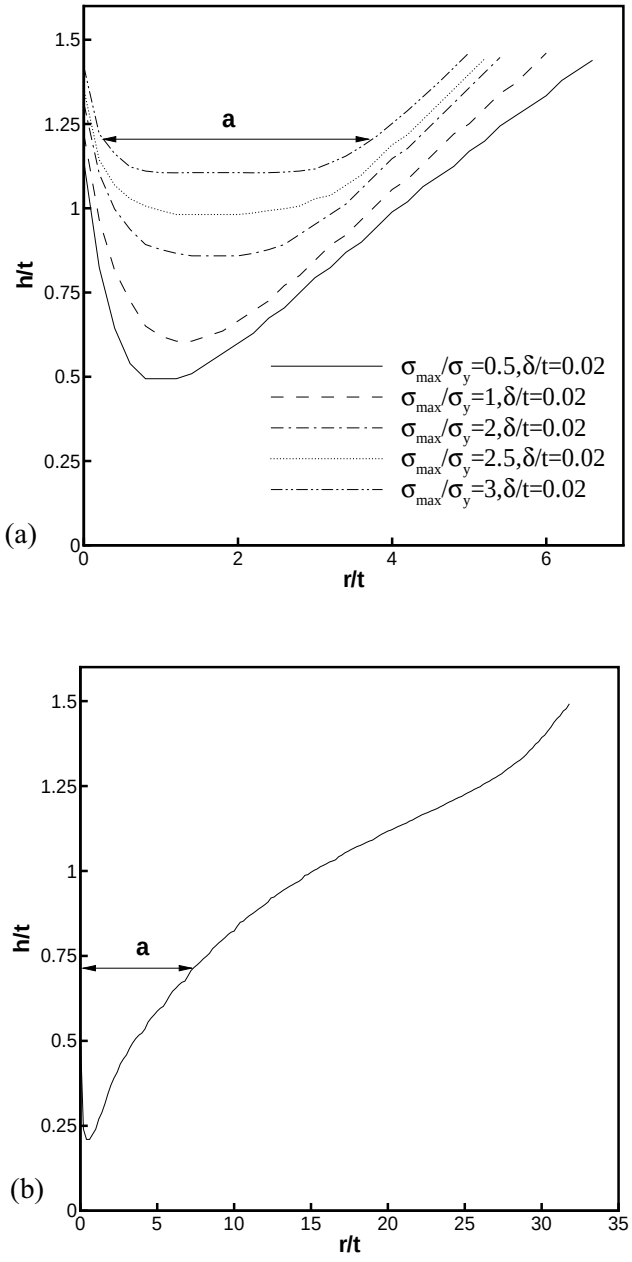

Figure 5 : Computed delamination extensions for (a) $\delta/t = 0.02$ and various values of σ_{max}/σ_y and (b) the weak interface with σ_{max}/σ_y=0.025 and $\delta/t = 0.005$.

is increased. Furthermore, for very strong interfaces the onset of delamination occurs over a considerable area of the interface, e.g. an interface ring between $r = t$ to r=3t in the case of σ_{max}/σ_y=3.0. Due to large amount of local unloading in the cohesive zone, such an initiation event is reflected in the pop-in behavior observed in the $(P-h)$ curves for strong interfaces.

Subsequent growth of the delaminations occurs in both r^+- and r^--direction, with the rate in r^+ considerable larger than in r^--direction. For all cases investigated, the film debonds completely under the indenter. The final delamination length for the strong interfaces is small and reaches only several times the film thickness. No growth of the delamination occurred during unloading.

Figure 5b depicts the development of the delamination for the weak interface case. Now, the onset of delamination occurs already at small indentation depths (h/t=0.15), with the site of nucleation remaining at $r = t$. Subsequently, the delamination again expands in both r^+-and r^--directions, but with the rate of growth being significantly larger in the r^+-direction.

Nevertheless, enough growth in r^-occurs such that the interface also delaminates directly under the indenter. The final radius of the delamination is equal to $32t$. Again, no growth of the delamination is observed during unloading.

The mode mixity at the current tip of the interface delamination growing in r^+-direction in dependence of the normalized indentation depth is given in Fig. 6. The mode mixity in the cohesive zone model is defined as the ratio of tangential to normal separation in the local coordinate system of the cohesive zone element at the current delamination tip:

$$\psi = \arctan\left(\frac{\Delta u_t}{\Delta u_n}\right) \tag{7}$$

In all cases the interface delamination initiates in pure shear ($\psi = 90°$), i.e. mode II conditions, due to the radial displacement mismatch in film and substrate. For the weak interface, ψ starts to deviate from $\psi = 90°$ abruptly as the delamination has extended as small amount. At this instance, the film buckles and the contribution of the normal separation becomes significant nearly instantaneously as the film lifts up from the substrate. The buckling event is accounted for in the numerical analysis without the use of any perturbation of the original mesh since the deformed shape of the film provides the required numerical perturbation. For the weak interface, ψ is predicted to decreases continuously, and passes $\psi = 0°$ as loading progresses. The mode mixity finally becomes negative for large h/t values as the radial stresses are being released due to the lift up of the film. For strong

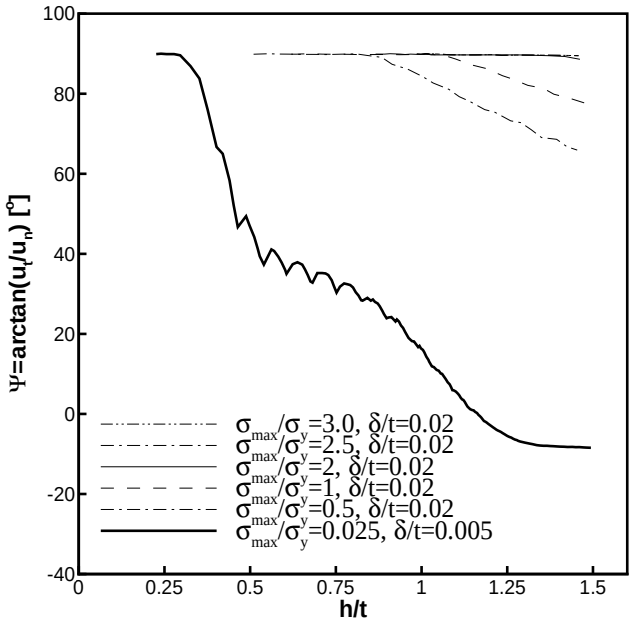

Figure 6 : Computed mode mixity in dependence of the indentation depth for δ/t=0.02 and various values of σ_{max}/σ_y, and the weak interface with σ_{max}/σ_y=0.025 and δ/t=0.005.

interfaces no distinct buckling event occurs, as already seen in the contour plots in Fig. 3ab. The delamination remains close to $\psi = 90^\circ$ up to large values of h/t. If the interface is very strong, the delamination remains in mode II up to the final indentation depth. For less strong interface, some mixed mode delamination growth occurs at large values of h/t. Nevertheless, the transition into the mixed mode delamination occurs much less abrupt than for the weak interface with buckling.

3.2 Interface Properties

For weak interfaces the analysis of indentation experiments of film-substrate systems is commonly based on an approach within linear elastic fracture mechanics applied to framework of film buckling as outlined in Marshall and Evans (1984). Thereby, the energy release rate at the tip of the delamination is given from a comparison between buckled and unbuckled configurations. The normalized energy release rate at the delamination tip is given by

$$\frac{G}{e t \sigma_y} = \frac{\sigma_I^2(1-\nu_f^2)}{2e\sigma_y E_f} - (1-\alpha)\frac{(\sigma_I-\sigma_B)^2(1-\nu_f)}{e\sigma_y E_f} \qquad (8)$$

Here, α is

$$\alpha = 1 - \left\{1/\left[1+0.9021(1-\nu_f)\right]\right\}, \qquad (9)$$

σ_I is the indentation induced stress at a given indentation volume,V_I:

$$\sigma_I = \frac{V_I E_f}{2\pi t a^2(1-\nu_f)} \qquad (10)$$

and σ_B is the critical stress for buckling of the film:

$$\sigma_B = \frac{\mu^2 E_f}{12(1-\nu_f^2)}\frac{t^2}{a^2} \qquad (11)$$

with μ^2=14.68 for single buckling and μ^2=42.67 for double buckling.

This framework is applied to the weak interface case discussed here. From the simulations the buckling event is defined to have occurred if the maximum normal separation along the interface becomes equal to 5δ. This condition is met at an indentation depth of h =0.524t, which corresponds to a delamination length of a =4.4t. With this value of crack length, Eq. 11 predicts a buckling stress as σ_B/E_f=0.24. From the finite element simulation, the radial stress in the film at the radius corresponding to the location of the delamination tip at buckling is σ_{rr}/E_f=0.0023. As can be seen from the contour plot of Fig. 3c, the plastic zone extends over the entire delamination at the instance of buckling. Film buckling is thus rather described by considerations of plastic buckling. In a first approximation, the effect of the plastic zone can be accounted for by substituting the film elastic properties, E_f and ν_f by the film hardening modulus, H_f and $\nu_{f,pl}$=0.5, leading to σ_B/E_f=0.00074. Thereby, elastic buckling is substituted by the lower bound of possible plastic buckling solutions, which seems reasonable since further loading after buckling occurs under increased load, as indentation continues [Shanley (1946)]. The remaining differences between computation and prediction buckling loads can be contributed to several factors, requiring further investigation. The boundary conditions of the film are complex, since it is supported by the cohesive zone with provides neither simple supports nor an ideal clamped configuration. In the buckling analysis the use of the instantaneous modulus and instantaneous compression ratio, Hutchinson (1974), might provide better predictions. Also, the presence of imperfections due to film and substrate deformation can influence the results.

Finally, the film thickness to delamination length ratio is small at buckling, such that buckling solutions accounting for shear stresses might be appropriate.

At the instance of film buckling Eq. 8 cannot be applied to determine the interface toughness – or cohesive energy –, neither under considerations of elastic nor plastic buckling. The delamination tip is embedded in the plastic zone which extents through the entire film thickness. Thus, large-scale yielding conditions are present, and the contribution of plastic dissipation and the work needed to actually separate the interface, cannot be accounted for individually.

Equation 8 was applied to analyze the computational results at the final delamination length where the delamination tip is far outside the plastic zone. The energy release rate from Eq. 8 is then calculated using the computed delamination length, $a = 32t$, at maximum indentation depth. With the indentation volume, V_I, given from the indentation depth under consideration of the cone geometry, Eq. 8 predicts $G/(et\sigma_y)$=1.5×10^{-3}. Since at final maximum indentation depth the tip of the delamination is disconnected from the plastic zone, Fig. 3d, a comparison of the prediction from Eq. 8 with the cohesive energy, $\phi_c/(et\sigma_y)$=1.25×10^{-4}, can be made. The energy release rate predicted by Eq. 8 is more then ten times larger than the value of the cohesive energy used as input in the simulation. There are several reasons that lead to this large difference. In Marshall and Evans (1984) growth of the delamination was not considered. In the computations, the final delamination is obtained as the result of a large amount of growth in the post-buckling state. Furthermore, the extension of the plastic zone was neglected in deriving Eq. 8. In the present computations, however, the plastic zone is responsible for the delamination formation, and its presence and extent cannot be neglected.

For the strong interfaces Eqs. 8 to 11 cannot provide information on the interface toughness since no buckling is present, and, more importantly, the film is deformed plastically in the volume at the current delamination tip such that a large scale yielding situation exists. Often, strong interfaces were excluded from indentation experiments [Kriese, Gerberich, and Moody (1999a)], or special provision were undertaken to increase the mechanical constraint on the film in order to reduce the amount of plastic deformation and obtain buckling [Bagchi and Evans (1996), Kriese, Gerberich, and Moody (1999b)]. In ductile fracture mechanics, it is well documented that the cohesive zone model approach is well suited to provide solutions for large scale yielding cases since the energy dissipation in the fracture process and the plastic zone are accounted for separately. For considerations within this context, see the paper by [Chandra and Shet (2004)] in this issue of CMES. For ductile crack growth the calibration of the cohesive zone parameters is performed in a two-step process. First the cohesive energy is calibrated on values of the measured crack initiation toughness, and subsequently the tearing modulus is used to find the cohesive strength [Tvergaard and Hutchinson (1996)].

Such a calibration methods for the determination of the cohesive zone parameters cannot be successfully applied to the indentation tests since large scale yielding already exists

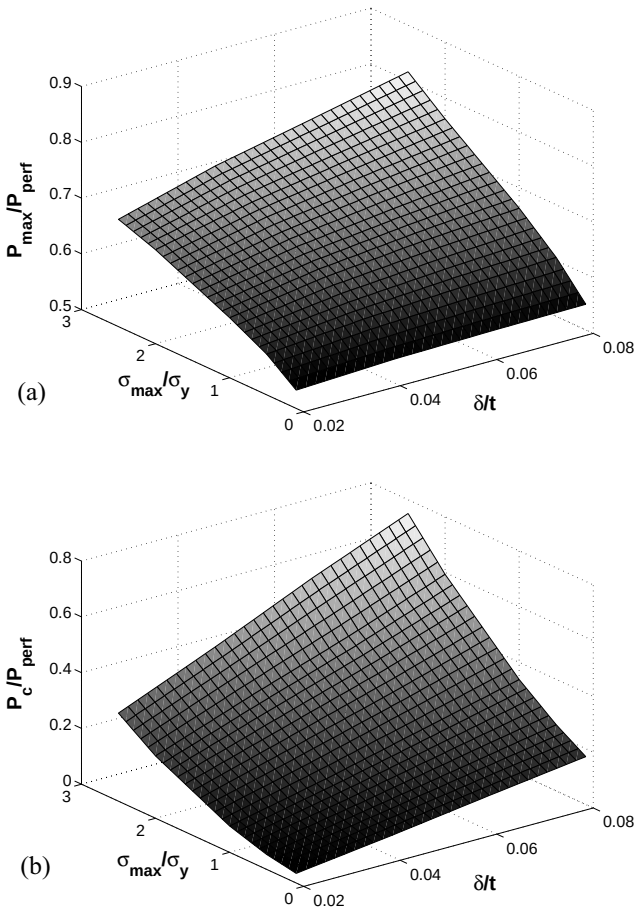

Figure 7 : Surface plots of the dependence of (a) P_c/P_{perf} and (b) P_{max}/P_{perf} on the cohesive zone parameters.

at the instance of delamination initiation. Based on the data of the computational study performed here, calibration charts are suggested such that the cohesive zone properties can be obtained from indentation experiments. The traction- separation law characterizing the cohesive zone possesses two parameters. Thus, to identify both of the two parameters from $(P-h)$ curve two critical data points are to be determined, i.e. the load P_c at which $(P-h)$ deviates from $(P-h)_{\text{perf}}$, as well as the maximum load, P_{max}. Values of P_c/P_{perf} and P_{max}/P_{perf} are depicted in Fig. 7a and b, respectively, in their dependence on the normalized cohesive zone parameters δ/t and σ_{max}/σ_y. As the interface becomes stronger, either by increasing δ/t or σ_{max}/σ_y, the value of both P_c/P_{perf} and P_{max}/P_{perf} increases. The data from Fig. 7a and b is replotted in the form of a contour plot in δ/t - σ_{max}/σ_y space, Fig. 8. It is assumed that P_c and P_{max} are known from an experiment on a film-substrate system with debonding, and P_{perf} is obtained from a reference experiment with a perfect interface or from simulations. For each pair of data $P_c/P_{\text{perf}} - P_{max}/P_{\text{perf}}$ a pair of intersecting lines can be identified in this contour plot. The coordinates of the intersection point are then the normalized cohesive zone properties characterizing the interface between film and substrate. A test simulation is performed to determine the accuracy of the interpolations applied to obtain the contour plot in Fig. 7. The simulation is performed with σ_{max}/σ_y=0.788 and δ/t=0.0268. The results of the finite element simulation were P_c/P_{perf}=0.097 and P_{max}/P_{perf}=0.602. These numbers are in good agreement with the results from Fig. 7 where P_c/P_{perf} =0.1 and P_{max}/P_{perf} =0.6 for these cohesive zone properties.

It can be observed that for large values of the cohesive energy the two families of curves belonging to P_c/P_{perf} and P_{max}/P_{perf}, respectively, intersect at a shallow angle. It can thus become difficult to accurately determine the cohesive properties from Fig. 8. In that case additional results obtained from the indentation experiment, e.g. the delamination length after unloading, can be used to complete the parameter identification. It shall finally be remarked here, that different forms of the traction-separation law might change the actual shape of the calibration chart.

4 Conclusions

A cohesive zone model is used to study the mechanics of indentation tests performed on systems consisting of a ductile film on an elastic substrate. Considerable differences exist in the delamination growth behavior in systems with weak and strong interfaces. For the weak interfaces considered, buckling and the subsequent growth of the buckled delamination occurs. For strong interfaces shear delamination dominates. The computations predict all these events to occur under considerable amounts of plastic deformation in the film. Large-scale yielding conditions exist both at the instance of film buckling for the weak interface, as well as for the shear delaminations. The commonly used framework based on elastic fracture mechanics cannot be used to determine the interface toughness in this case. As an alternative, for the strong interfaces, the use of calibration charts for the determination of the interface properties is suggested.

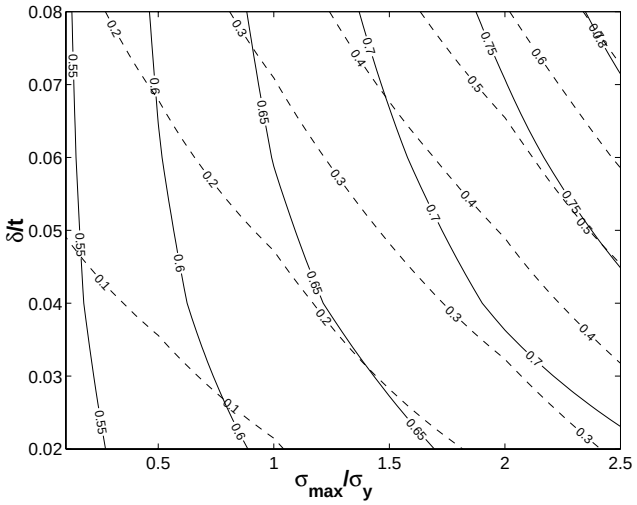

Figure 8 : Contour plots of P_c/P_{perf}(- - - -) and P_{max}/P_{perf} (——) in dependence of the cohesive zone parameters.

Acknowledgement: Support by Purdue Research Foundation via a fellowship to W.L. is acknowledged.

References

Abdul-Baqi, A.; Van der Giessen, E. (2001a): Indentation-induces interface delamination on a strong film on a ductile substrate. *Thin Solid Film*, vol. 381 pp. 143-154.

Abdul-Baqi, A.; Van der Giessen, E. (2001b): Delamination of a strong film from a ductile substrate during indentation unloading. *J Mater Res*, vol. 16(5) pp.1396-

1407.

Abdul-Baqi, A.; Van der Giessen, E. (2002): Numerical analysis of indentation-induced cracking of brittle coatings on ductile substrates. *Int J of Solids Struct*, vol. 39(6) pp. 1427-1442.

Bagchi, A.; Evans, A. G. (1996): Measurements of the debond energy for thin metallization lines on dielectrics, *Thin Solid Films*, vol. 286(1-2) pp.203-212.

Chandra, N.; Shet, C. (2004): A Micromechanistic Perspective of Cohesive Zone Approach in Modeling Fracture, *CMES: Computer Modeling in Engineering & Sciences*, Vol. 5, No. 1, pp. 21-33.

Hutchinson, J. W. (1974): Plastic buckling. *Adv. Appl. Mech*, vol. 14, pp. 67-144.

Kriese, M. D.; Moody, N. R.; Gerberich, W. W. (1998): Effect of annealing and interlayers on the adhesion energy of copper thin film to SiO_2/Si substrate. *Acta Mater*, vol. 46(18), pp. 6623-6630.

Kriese, M. D.; Gerberich, W. W.; Moody N. R. (1999a): Quantitative adhesion measures of multilayer films: Part I. Indentation mechanics. *J Mater Res*, vol. 14(7) pp. 3007-3018.

Kriese, M. D.; Gerberich, W. W.; Moody N. R. (1999b): Quantitative adhesion measures of multilayer films: Part II. Indentation of W/Cu, W/W, Cr/W. *J Mater Res*, vol. 14(7) pp. 3019-3026.

Lemaitre, J. (1996): A course in damage mechanics. Springer, Berlin Heidelberg.

Malzbender, J.; de With, G. (2000): Energy dissipation, fracture toughness and the indentation load-displacement curve of coated materials. *Surf Coat Techn*, vol. 135(1) pp. 60-68.

Maiti, S.; Geubelle, P. H. (2004): Mesoscale Modeling of Dynamic Fracture of Ceramic Materials, *CMES: Computer Modeling in Engineering & Sciences*, Vol. 5, No. 2, pp. 91-101.

Marshall, D. B.; Evans, A. G. (1984): Measurement of adherence of residually stressed thin-films indentation 1. Mechanics of interface delamination. *J Appl Phys*, vol. 56(10) pp. 2632-2638.

Shanley, F. R. (1946): The column paradox, *J Aero Sci*, vol. 13(12) pp. 678.

Tvergaard. V.; Hutchinson, J. W. (1996): Effect of strain-dependent cohesive zone model on predictions of crack growth resistance, *Int J Solids Struct*, vol. 33(20-22) pp. 3297-3308.

Volinsky, A. A.; Moody, N. R.; Gerberich, W. W. (2002): Interfacial toughness measurements for thin films on substrates. *Acta Mater*, vol. 50, pp. 441-466.

Zhang, P.; Klein, P.; Huang, Y.; Gao, H.; Wu, P. D. (2002): Numerical simulation of cohesive fracture by the virtual-internal-bond model. *CMES: Computer Modeling in Engineering & Sciences*, vol. 3(2) pp. 263-278

Zhang, Y. W.; Zeng, K. Y.; Thampurum R. (2001): Interface delamination generated by indentation in thin film system – A computational mechanics study. *Mat Sci Eng*, vol. 319A-321A pp. 893-897.